THE 1918/19 EL NIÑO

BY BENJAMIN S. GIESE, GILBERT P. COMPO, NIALL C. SLOWEY, PRASHANT D. SARDESHMUKH, JAMES A. CARTON, SULAGNA RAY, AND JEFFREY S. WHITAKER

An ocean model forced with winds from an atmospheric reanalysis of the first half of the twentieth century shows that the 1918/19 El Niño was much stronger than previously thought.

By any measure the year 1918 was tumultuous. Marked by the end of World War I, an influenza pandemic that killed over 25 million people (Johnson and Mueller 2002), a crippling drought in India (Parthasarathy et al. 1994), and revolutions in four countries, it was a period of tremendous social upheaval. It was also a year of intense global climate variability. The year 1918 began with record-setting cold temperatures in much of the United States: January 1918 still stands as the coldest January registered in Central Park in New York, New York. In summer, just as influenza started to take hold in the

AFFILIATIONS: GIESE, SLOWEY, AND RAY—Department of Oceanography, Texas A&M University, College Station, Texas; COMPO AND SARDESHMUKH—University of Colorado/CIRES Climate Diagnostics Center, and NOAA/Earth Systems Research Laboratories/Physical Sciences Division, Boulder, Colorado; CARTON—Department of Atmospheric and Oceanic Sciences, University of Maryland, College Park, College Park, Maryland; WHITAKER—NOAA/Earth Systems Research Laboratories/Physical Sciences Division, Boulder, Colorado
CORRESPONDING AUTHOR: Benjamin S. Giese, Department of Oceanography, Texas A&M University, College Station, TX 77843
E-mail: b-giese@tamu.edu

trenches of eastern Europe, India began to experience one of its worst droughts of the twentieth century (Parthasarathy et al. 1994). Late summer and fall were marked by an unusually weak Atlantic hurricane season (Donnel 1918), and in late fall North America was unusually warm.

Climate patterns such as a weak Atlantic hurricane season, failure of the Indian monsoon, and weak all-Australia rainfall are widely recognized as El Niño teleconnections (Gray 1984; Torrence and Webster 1999; Power et al. 2006). However, Quinn et al. (1987) describe the El Niño of 1918 as "weak to moderate" and Kaplan et al. (1998) show modest temperature anomalies of about only 3°C in December 1918 with the largest anomalies adjacent to the coast of South America. It is difficult to reconcile the strong global teleconnections with a tepid El Niño; however, there is some evidence that ocean temperatures in the east Pacific may not have captured the intensity of the 1918/19 El Niño. Quinn et al. draw a distinction between El Niño, which they take to mean the oceanic changes that occur near the coast of South America, and El Niño–Southern Oscillation (ENSO), which they take to mean basin-scale ocean–atmosphere changes. Interestingly, in an earlier paper, Quinn et al. (1978) rank the 1918/19 ENSO, which includes indicators such as the Southern Oscillation index (SOI) and precipitation anomalies throughout the Pacific basin, as strong. In this paper, we consider El Niño and ENSO to refer to the same coupled phenomenon.
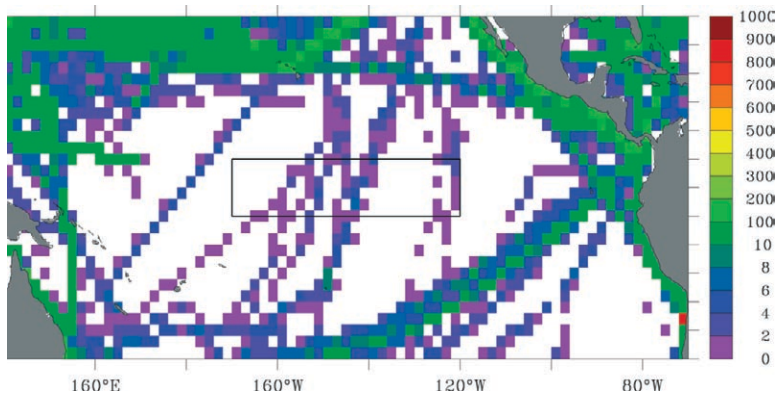
FIG. 1. The number of surface temperature observations in the ICOADS (Worley et al. 2005) dataset from Jan 1918 through Dec 1919. Note the limited number of observations in the Niño-3.4 region (shown as a rectangle).

A lack of ocean observations from the central equatorial Pacific during the first half of the twentieth century has limited efforts to determine the strength of El Niño prior to the late 1950s. A difficulty in characterizing the severity of past El Niño events is that there are few direct observations of the tropical Pacific Ocean available for this purpose. The number of sea surface temperature (SST) observations in the International Comprehensive Ocean Atmosphere Data Set (ICOADS; Worley et al. 2005) for the years of 1918 through 1919 is shown in Fig. 1. Shown by a rectangle is the Niño-3.4 region, which extends from 5°S to 5°N and from 170° to 120°W and is a commonly used measure of El Niño intensity. Note that the number of SST observations in the Niño-3.4 region during this 2-yr period is extremely limited, but there are regions along the coast of South America for which the data coverage is better. The principal reason that there are few direct measurements in the central Pacific Ocean during this period is that the war effort concentrated shipping, and hence the ability to measure SST, in the North Atlantic. A similar reduction of observations occurs during World War II.

As a result of limited observations, scientists often rely on SST reconstructions (Kaplan et al. 1998; Rayner et al. 2003), which combine temporal records of SST at a few locations with typical spatial patterns of SST observed in later decades that have more abundant data. A limitation of this methodology is that it assumes that the spatial patterns of

SST variability do not change over time. An alternative method is to use an ocean model to "hindcast" the SST fields. Until recently it was not possible to model the state of the tropical Pacific Ocean before the 1950s, primarily because of the lack of surface meteorological forcing data. However, a new reanalysis dataset of the atmospheric circulation for the period of 1908 through 1958 provides us with this missing atmospheric forcing dataset, and allows us to model the ocean state in the first half of the twentieth century.

This study relies on an ocean hindcast, which we refer to as SIMU 3.0.2, of the global oceans from 1908 through 1958. The ocean model is based on the Parallel Ocean Program (POP) software (Smith et al. 1992). The ocean model has a global average 0.25° (latitude) × 0.4° (longitude) × 40-level eddy-permitting resolution with 10-m spacing near the surface.

The ocean model surface boundary conditions are provided from a new atmospheric dataset called the Twentieth Century Reanalysis Project (C20r; Whitaker et al. 2004; Compo et al. 2006, 2008). These atmospheric reanalyses include only surface observations of synoptic pressure and monthly SST and sea ice distribution from the Hadley Centre Global Sea Ice and Sea Surface Temperature, version 1.1 (HadISST1.1) dataset (Rayner et al. 2003). The atmosphere reanalysis uses a state-of-the-art data assimilation methodology called the ensemble filter, which is described by Whitaker and Hamill (2002). The surface wind stress from C20r is used in the ocean model for the surface momentum fluxes.
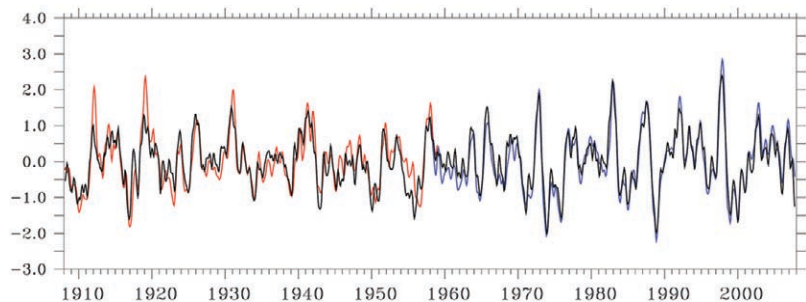

FIG. 2. Niño-3.4 index time series (°C) based on reconstructed SST (black), simulated SST (red), and ocean reanalysis SST (blue). Anomalies were computed by removing the monthly climatology from 1908 to 2007 for HadISST1.1, from 1908 to 1958 for the simulation, and from 1958 for 2007 for the ocean reanalysis.

Solar radiation, specific humidity, cloud cover, 2-m air temperature, precipitation, and 10-m wind speed are used in the bulk formulas for computing heat and freshwater fluxes. Model output, such as temperature, salinity, and velocity, is averaged by month and is mapped onto a uniform global 0.5° (latitude) × 0.5° (longitude) × 40-level (vertical) grid using the horizontal grid spherical coordinate remapping and interpolation package, with second-order conservative remapping (Jones 1999).

The Niño-3.4 temperature anomaly from the HadISST1.1 reconstruction is shown for the period from 1908 through 2007 in Fig. 2 as a black curve. The Niño-3.4 reconstruction shows a succession of El Niño and La Niña events, with amplitudes that range from fairly weak (particularly in the early part of the record) to very strong (notably in 1982/83 and 1997/98). However, the number of observations that go into this Niño-3.4 SST reconstruction are quite limited in the first half of the twentieth century (Fig. 1); notably, there were few direct observations of temperature during the period from 1917 through 1919. Thus, during these early years the Niño-3.4 SST reconstruction relies heavily on assumed geographic patterns together with SST observations outside of the Niño-3.4 region, and thus it should be assumed to be tentative.

Also shown in Fig. 2 is the simulated Niño-3.4 SST anomaly for the period from 1908 through 1958 from SIMU 3.0.2 (in red) and the Niño-3.4 SST anomaly from an ocean reanalysis (Carton and Giese 2008) for the period from 1958 to 2007. In the latter part of the twentieth century, when there are many observations, the reconstructed Niño-3.4 SST and the reanalyzed Niño-3.4 SST agree quite well. However, in the early part of the record there is a considerable difference in estimation of the magnitude of El Niño events, even though the two time series are well correlated ($r = 0.86$). Of particular interest

is the SST anomaly during the 1918/19 El Niño, for which the reconstructed SST suggests a fairly modest El Niño with an anomaly of about 1.5°C, while simulated SST reveals the presence of a massive event with Niño-3.4 SST anomalies in excess of 2.5°C.

To confirm our estimates of the strength of the 1918 El Niño, we first turn to an indirect proxy, the ratio of the ^{18}O to ^{16}O isotopes in tropical Pacific corals whose isotope ratio changes with changing surface temperature and salinity (Cole et al. 1993). The coral isotope record (expressed in $\delta^{18}O$ notation) from the Maiana Atoll (0.93°N, 173°W; Urban et al. 2000) in the central equatorial Pacific is in excellent overall agreement with the simulated Niño-3.4 time series (Fig. 3). The two time series have a correlation
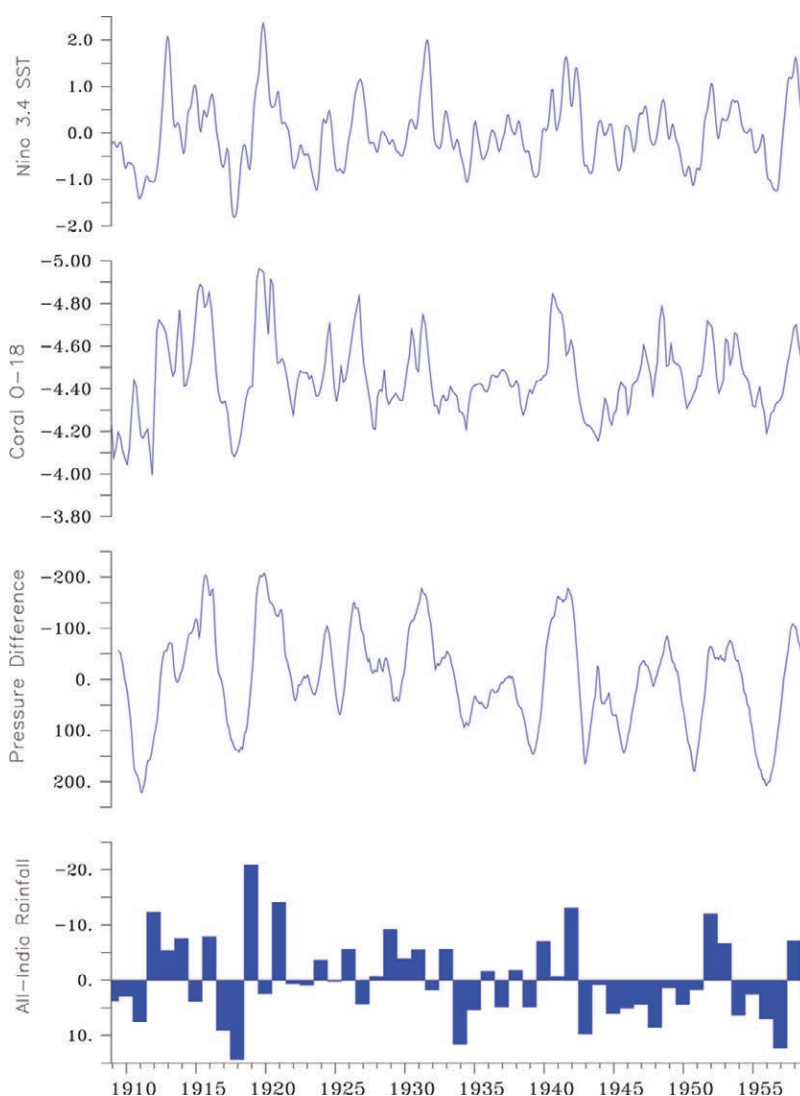

F𝐼G. 3. Simulated Niño-3.4 index time series (as in Fig. 2), Maiana Atoll $\delta^{18}O$ isotopic anomaly time series (Urban et al. 2000), the C20r Tahiti–Darwin difference of surface pressure (Pa), and the all-India seasonal (Jun–Sep) rainfall anomaly (cm; Parthasarathy et al. 1994).

of $r = 0.68$. There is a high degree of coherence between $\delta^{18}O$ and the Niño-3.4 temperature anomaly in the period from 1917 through 1919, with the highest temperature anomaly from the simulation coinciding with the lowest value of $\delta^{18}O$ and the lowest temperature anomaly coinciding with one of the highest values of $\delta^{18}O$.

The surface pressure difference between Tahiti and Darwin (akin to the SOI) from the C20r reanalysis is plotted in the third panel from the top. This pressure difference, an important measure of interannual variability, has been smoothed with a 12-month running average. The pressure difference shows that 1918/19 is anomalous, as expected during an El Niño event. However, the pressure difference from the C20r run is not as exceptional during 1918/19 as the SST anomaly is from the ocean simulation. An equally large SOI

anomaly occurs during 1915, even though the SST anomalies are weak at this time.

Failure of the Indian monsoon, one of the reasons that Sir Gilbert Walker first started exploring changes in the climate of the Pacific in the nineteenth century, is intimately linked to El Niño (Torrence and Webster 1999). Krishna Kumar et al. (1999) show that the relationship between ENSO and the Indian monsoon varies decadally, but they show that in the early part of the twentieth century the relationship is strong. Precipitation averaged over India from the Dai et al. (1997) dataset shows a striking change between 1917 and 1918, when rainfall went from well above normal, to well below normal (Fig. 3, lower panel). In fact, 1918 is recognized as one of the most severe droughts of the Indian subcontinent during the twentieth century, matched only by the intense drought of 1972 (also a year of a strong El Niño, e.g., Fig. 2). Maps of precipitation anomalies show that during the El Niño event there were negative anomalies over much of India, over the west and east parts of Australia, and over the Nordeste region of Brazil. There are positive anomalies over much of Southeast Asia and the Gulf states of North America. Island precipitation data show that central and western Pacific rainfall was extremely high in late 1918 and early 1919 (Ichiye and Petersen 1964; Reiter 1978), consistent with a strong El Niño.

The evolution of wind and SST anomalies during the 1918 event, shown in Fig. 4, is consistent with that of a strong El Niño (Harrison and Larkin 1998). Throughout most of 1917 stronger-than-normal easterly trade winds forced anomalously strong upwelling and colder-than-normal SST. Many El Niño events are thought to be initiated by intense mesoscale
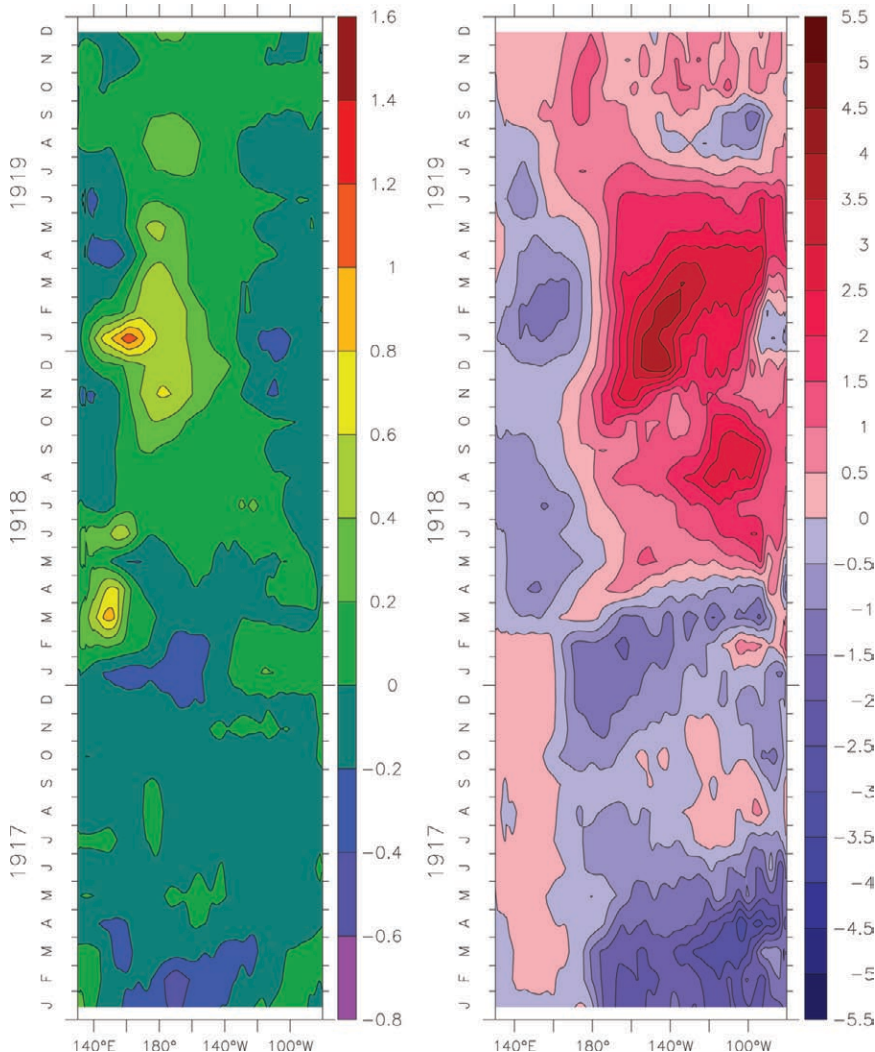

FIG. 4. Time–longitude anomalies relative to the climatology from 1908 to 1958 of the equatorial Pacific climate averaged over 2.5°S–2.5°N during 1917–19. (a) Zonal wind stress anomaly (dynes cm⁻²) and (b) simulated SST anomaly (°C).
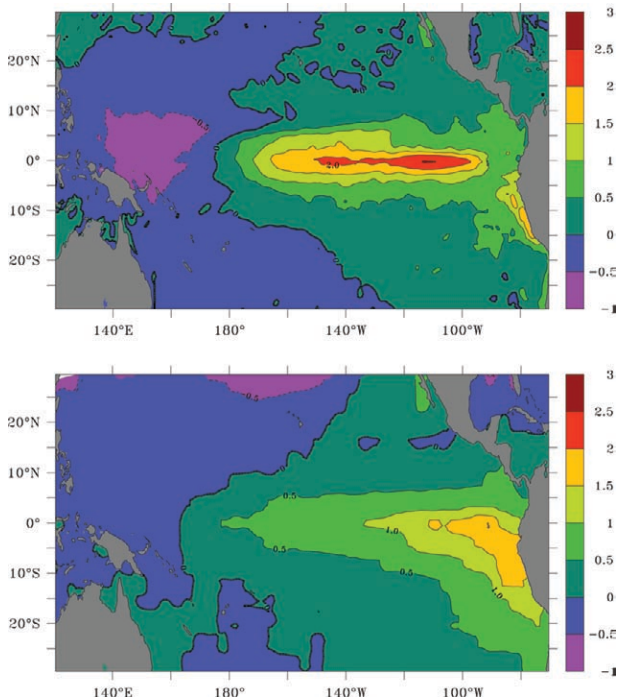
FIG. 5. SST anomaly (°C) averaged for the period from Apr 1918 through May 1919 from the (top) simulation and (bottom) HadISST1.1 dataset. A climatology for the period from 1908 to 1958 is removed to form the anomaly.

convective events in the western equatorial Pacific, known as westerly wind bursts (Giese and Harrison 1990). In March 1918 an intense westerly wind burst occurred with peak zonal stress of 0.75 N m⁻². It is interesting to note that the intensity of this wind burst exceeds that of the westerly wind bursts preceding the 1997/98 El Niño, which are shown by McPhaden (1999). The March 1918 westerly wind burst, and a somewhat weaker wind event in June and July 1918, led to surface warming (Fig. 4, right-hand panel). The warming spreads eastward across the Pacific through the spring and early summer of 1918, reaching the coast of South America in May 1918. In the central Pacific the warming continued until about September 1918 and then began to abate.

Beginning in late September 1918 there is another period of westerly wind anomalies, peaking in January 1919 with another strong episode of westerly wind. This weakening of the easterly trade winds in fall and winter of 1918/19, as well as the in-

tense westerly wind episode, led to an even stronger warming of the surface (in excess of 4°C) from November 1918 through March 1919. By July 1919 the eastern equatorial Pacific had cooled to below normal, although interestingly there were still weak westerly wind anomalies in the western Pacific.

That the strength of the 1918/19 El Niño was not previously recognized is likely due to two factors. The first is the fact that during World War I the number of ocean observations was extremely low, so that at the peak of the El Niño there were few SST measurements in the Niño-3.4 region. The second is the fact that the 1918/19 El Niño had only a relatively weak expression near the coast of South America. The SST anomaly averaged from April 1918 through May 1919, the period of warming during the 1918/19 El Niño, is shown from the simulation (Fig. 5, upper panel) and from the HadISST1.1 reconstruction (lower panel). The simulation shows a strong SST anomaly from 160° to 90°W and a weaker warming near the coast of South America. The HadISST1.1 reconstruction shows the largest SST anomaly adjacent to the coast of South America, with modest warming in the central Pacific. Because the few observations that were taken in 1918/19 were near the coast of South America, SST reconstructions tend to underestimate this El Niño. This result may also explain the incongruity of Quinn et al. (1987) ranking the 1918/19 El Niño as weak to moderate, whereas earlier the 1918 ENSO was ranked as strong (Quinn et al. 1978).

Did the 1918/19 El Niño play a role in the events that unfolded during 1918? It seems likely that this El Niño was responsible for the failure of the summer monsoon that afflicted India. Krishna Kumar et al.
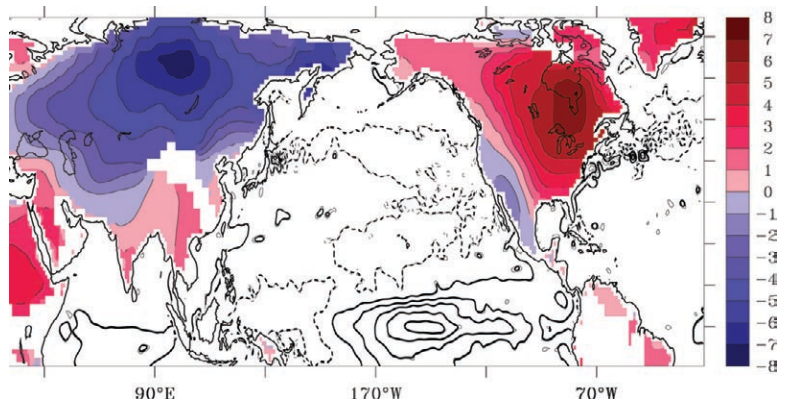

FIG. 6. The change in boreal winter (DJF) climate from 1917/18 to 1918/19. Values over land are shaded in 1°C intervals and come from the NASA Goddard Institute for Space Studies surface air temperature (Hansen et al. 1999) dataset and values in the oceans are from the ocean simulation. The contour interval for SST is 1°C, starting at 0.5°C.

(1999) show that the relationship between El Niño and the failure of the Indian monsoon has changed, with a stronger relationship in the period from 1860 to 1970. Unlike El Niño in recent decades, the 1918/19 event was confined to the central portion of the Pacific Ocean (Fig. 5, upper panel) and did not have a strong east Pacific signature. Thus, the trans-Niño index (TNI; Trenberth and Stepaniak 2001) for the 1918/19 El Niño is relatively weak. It has been shown that El Niño events with weak TNI are more likely to be associated with drought in India (Krishna Kumar et al. 2006). Our results fit well with that finding: The 1918/19 event is a very strong El Niño as measured by the Niño-3.4 index, but has a weak TNI, and the 1918 Indian drought was one of the strongest of the twentieth century. It is also notable that influenza, which coincided with the anomalous changes in global climate, hit the Indian population particularly hard that summer, with mortality estimated at 18 million people (Johnson and Mueller 2002). The coincidence of these events suggests that climate may have played a role in the devastating mortality of the 1918 influenza pandemic in India.

One expects such dramatic changes in the equatorial Pacific to have consequences for climate over North America. The winter [December–February (DJF)] surface air temperature (Hansen et al. 1999) difference between 1917/18 and 1918/19 over land is shown in Fig. 6. The winter SST change between 1917/18 and 1918/19 from our simulation is shown as contours. Surface air temperature warmed by 8°C in eastern North America, with some cooling in the southwest United States and northern Mexico. Similarly dramatic changes in climate occurred across much of central northern Asia. Indeed, the surface air temperature change from 1917/18 to 1918/19 is among the largest year-to-year changes on record.

This study raises several questions about our understanding of El Niño and a changing climate. These questions include understanding how El Niño changes both on decadal time scales and in response to global warming. The model results suggest that El Niño events in the beginning of the twentieth century were comparable in magnitude to the strong events in 1982/83 and 1997/98, raising the possibility that El Niño strength has not increased significantly in response to global warming. However, the model results do show that El Niño events were stronger at the beginning and end of the twentieth century, with weaker events in the middle of the twentieth century (Fig. 2). Because the twentieth-century reanalysis uses the HadISST1.1 data as a surface

boundary condition, there is the possibility that the atmospheric response of the C20r reanalysis is underestimated. Future studies are planned to explore the atmospheric response to modeled SST because the model-generated SST would, in principle, give rise to a stronger atmospheric response to the larger SST anomalies. The methodology used in this paper could also be used to understand other strong, but poorly observed, El Niño events, such as the 1939–41 and 1912 El Niños.

REFERENCES

Carton, J. A., and B. S. Giese, 2008: A reanalysis of ocean climate using simple ocean data assimilation (SODA). *Mon. Wea. Rev.*, **136**, 2999–3017.

Cole, J. E., R. G. Fairbanks, and G. T. Shen, 1993: Recent variability in the Southern oscillation: Isotopic results from a Tarawa Atoll coral. *Science,* **260**, 1790–1793.

Compo, G. P., J. S. Whitaker, and P. D. Sardeshmukh, 2006: Feasibility of a 100-year reanalysis using only surface pressure data. *Bull. Amer. Meteor. Soc.*, **87**, 175–190.

——, ——, and ——, 2008: The 20th century reanalysis project. *Proc. Third WCRP Int. Conf. on Reanalysis,* Tokyo, Japan, WCRP. [Available online at http://wcrp.ipsl.jussieu.fr/Workshops/Reanalysis2008/Documents/V5-511_ea.pdf.]

Dai, A., I. Y. Fung, and A. D. Del Genio, 1997: Surface observed global land precipitation variations during 1900–1988. *J. Climate*, **10**, 2943–2962.

Donnel, C. A., 1918: Notes on hurricanes of 1918. *Mon. Wea. Rev.*, **46**, 568.

Giese, B. S., and D. E. Harrison, 1990: Aspects of the Kelvin wave response to episodic wind forcing. *J. Geophys. Res.*, **95**, 7289–7312.

Gray, W. M., 1984: Atlantic seasonal hurricane frequency. Part I: El Niño and 30-mb quasi-biennial oscillation influences. *Mon. Wea. Rev.*, **112**, 1649–1668.

Hansen, J., R. Ruedy, J. Glascoe, and M. Sato, 1999: GISS analysis of surface temperature change. *J. Geophys. Res.*, **104,** 30 997–31 022.

Harrison, D. E., and N. K. Larkin, 1998: El Niño–Southern Oscillation sea surface temperature and wind anomalies 1946–1993. *Rev. Geophys.*, **36**, 353–399.

Ichiye, T., and J. R. Petersen, 1963: The anomalous rainfall of the 1957–58 winter in the equatorial central Pacific arid area. *J. Meteor. Soc. Japan,* **41**, 172–182.

Johnson, N. P. A. S., and J. Mueller, 2002: Updating the accounts: global mortality of the 1918–1920 "Spanish" influenza pandemic. *Bull. Hist. Med.*, **65**, 105–115.

Jones, P. W., 1999: First- and second-order conservative remapping schemes for grids in spherical coordinates. *Mon. Wea. Rev.*, **127**, 2204–2210.

Kaplan, A., M. Cane, Y. Kushnir, A. Clement, M. Blumenthal, and B. Rajagopalan, 1998: Analyses of global sea surface temperature 1856–1991. *J. Geophys. Res.*, **103**, 18 567–18 589.

Krishna Kumar, K., B. Rajagopalan, and M. Cane, 1999: On the weakening relationship between the Indian monsoon and ENSO. *Science,* **284,** 2156–2159.

——, ——, M. Hoerling, B. Bates, and M. Cane, 2006: Unraveling the mystery of Indian monsoon failure during El Niño. *Science,* **314,** 115–119.

McPhaden, M. J., 1999: Genesis and evolution of the 1997–98 El Niño. *Science,* **283**, 950–954.

Parthasarathy, B., A. A. Munot, and D. R. Kothawale, 1994: All-India monthly and seasonal rainfall series: 1871–1993. *Theor. Appl. Climatol.,* **49**, 217–224.

Power, S., M. Haylock, R. Colman, and X. Wang, 2006: The predictability of interdecadal changes in ENSO activity and ENSO teleconnections. *J. Climate,* **19,** 4755–4771.

Quinn, W. H., D. O. Zopf, K. S. Short, and R. T. Kuo Yang, 1978: Historical trends and statistics of the Southern Oscillation, El Nino, and Indonesian droughts. *Fish. Bull.*, **76**, 663–678.

——, V. T. Neal, and S. A. Antunez de Mayola, 1987: El Niño occurrences over the past four and a half centuries. *J. Geophys. Res.*, **92**, 14 449–14 461.

Rayner, N. A., D. E. Parker, E. B. Horton, C. K. Folland, L. V. Alexander, D. P. Rowell, E. C. Kent, and A. Kaplan, 2003: Global analyses of sea surface temperature, sea ice, and night marine air temperature since the late nineteenth century. *J. Geophys. Res.*, **108**, 4407, doi:10.1029/2002JD002670.

Reiter, E. R., 1978: Long-term wind variability in the tropical Pacific, its possible causes and effects. *Mon. Wea. Rev.*, **106**, 324–330.

Smith, R. D., J. K. Dukowicz, and R. C. Malone, 1992: Parallel ocean general circulation modeling. *Physica D,* **60**, 38–61.

Torrence, C., and P. J. Webster, 1999: Inderdecadal changes in the ENSO–monsoon system. *J. Climate,* **12**, 2679–2690.

Trenberth, K. E, and D. P. Stepaniak, 2001: Indices of El Niño evolution. *J. Climate*, **14**, 1697–1701.

Urban, F. E., J. E. Cole, and J. T. Overpeck, 2000: Influence of mean climate change on climate variability from a 155-year tropical Pacific coral record. *Nature,* **407**, 989–993.

Whitaker, J. S., and T. M. Hamill, 2002: Ensemble data assimilation without perturbed observations. *Mon. Wea. Rev.*, **130**, 1913–1924.

——, G. P. Compo, X. Wei, and T. M. Hamill, 2004: Reanalysis without radiosondes using ensemble data assimilation. *Mon. Wea. Rev.,* **132,** 1190–1200.

Worley, S. J., S. D. Woodruff, R. W. Reynolds, S. J. Lubker, and N. Lott, 2005: ICOADS release 2.1 data and products. *Int. J. Climatol.*, **25**, 823–842.